Journal of Applied Physics

Mechanical properties of monolayer ternary transitional metal dichalogenides $MoS_{2x}Te_{2(1-x)}$: A molecular dynamics study

Cite as: J. Appl. Phys. **126**, 215105 (2019); https://doi.org/10.1063/1.5122264
Submitted: 03 August 2019 . Accepted: 09 November 2019 . Published Online: 02 December 2019

Penghua Ying, Jin Zhang, and Zheng Zhong

Journal of Applied Physics ARTICLE scitation.org/journal/jap

Mechanical properties of monolayer ternary transitional metal dichalogenides $MoS_{2x}Te_{2(1-x)}$: A molecular dynamics study

Cite as: J. Appl. Phys. **126**, 215105 (2019); doi: 10.1063/1.5122264
Submitted: 3 August 2019 · Accepted: 9 November 2019 ·
Published Online: 2 December 2019

Penghua Ying,[a] Jin Zhang,[a] and Zheng Zhong[b]

AFFILIATIONS

School of Science, Harbin Institute of Technology, Shenzhen 518055, People's Republic of China

[a]**Contributions:** P. Ying and J. Zhang contributed equally to this work.
[b]**Author to whom correspondence should be addressed:** zhongzheng@hit.edu.cn

ABSTRACT

In this paper, the mechanical behaviors of recently synthesized monolayer ternary transitional metal dichalogenides (TMDs) $MoS_{2x}Te_{2(1-x)}$ $(0 < x < 1)$ under tensile loading are studied by classical molecular dynamics simulations. Particular attention is paid to the fundamental mechanical properties such as Young's modulus and fracture behaviors of monolayer $MoS_{2x}Te_{2(1-x)}$. Our results show that Young's modulus of monolayer $MoS_{2x}Te_{2(1-x)}$ remains almost unchanged when the stoichiometric coefficient x is in the range of 0–0.4 but increases apparently when x increases from 0.4 to 1. In terms of their fracture behaviors, the alloyed ternary TMDs are found to show a ductile fracture feature, which is distinctly different from the brittle fracture behavior observed in their pristine binary TMD counterparts. The ultimate strength of alloyed ternary TMDs is found to be much lower than that of the pristine binary TMDs, which is attributed to the unaccommodated deformation caused by the stress concentration between Te atoms and nearby S atoms. The influence of loading direction and temperature on the aforementioned mechanical properties is also examined. It is found that Young's modulus and the ultimate strength of monolayer $MoS_{2x}Te_{2(1-x)}$ generally decrease with increasing temperature due to the temperature-induced softening effect. In the biaxial tensile test, Young's modulus and ultimate strength are found to be isotropic. The aforementioned mechanical parameters of monolayer $MoS_{2x}Te_{2(1-x)}$ under biaxial loading are significantly smaller than those under uniaxial loading. The present work is expected to significantly expand the knowledge of the mechanics of ternary TMDs and facilitate their applications in bandgap engineering.

I. INTRODUCTION

Two-dimensional (2D) materials exhibit superior physical properties and thus have great application potentials due to their reduced dimensions to monoatomic thickness. Graphene, as the first discovered 2D material,[1] has been found to be the strongest material ever measured,[2] which simultaneously exhibits excellent thermal and electrical conductivity.[3] Consequently, graphene has attracted intensive interest in the field of nanomaterials and nanotechnology for more than a decade.[4–8] Inspired by the superior physical properties of graphene, many researchers have commenced to focus on other similar 2D materials, most of which are found to possess unique physical properties different from graphene.[9,10] For example, most typical transitional metal dichalogenides (TMDs) such as MoS_2 and $MoTe_2$ naturally have a wide direct bandgap[11] and hence can be treated as a semiconductor, which is distinctly different from the intrinsic zero bandgap in graphene.[12] Other distinct material properties in TMDs, such as the phenomena of valley polarization[13,14] and quantum spin Hall effect,[15,16] are also reported very recently. These unique physical properties and phenomena different from graphene make TMDs a promising material for future device applications.[17]

Similar to graphene, the TMDs have weak out-of-plane van der Waals interactions and thus can be further exfoliated into 2D layers of single unit cell thickness.[1,18] However, atomic structures of these two materials are significantly different. Graphene contains only carbon atoms in the form of a hexagonal lattice with one-atom thickness, while TMDs, composed of two types of atoms (metal and oxide-group atoms), have more complicated atomic structures: each metal atom is surrounded by six oxide-group atoms and the metal atom layer is sandwiched by two oxide-group atom

layers.[19] This unique binary structure of TMDs makes it possible to synthesize ternary TMDs by replacing some of the metal atoms or the sulfide group atoms with other types of atoms.[20–23] Thus, by changing the stoichiometric coefficients of ions and anions in ternary TMDs, it is expected to achieve a way of efficiently tuning their physical properties, specifically the electrical properties. For instance, the bandgap engineering and phase controlling have been implemented in ternary TMDs $MoS_{2x}Se_{2(1-x)}$,[24,25] $WS_{2x}Se_{2(1-x)}$,[26] $W_xMo_{1-x}S_2$,[27] $Mo_{1-x}R_xSe_2$,[28] etc. Recently, 11 novel ternary TMDs were synthesized through molten-salt-assisted chemical vapor deposition,[21] which greatly expand the family of ternary TMDs. Despite the fact that the electrical properties of ternary TMDs have been widely investigated,[24–26] not enough attention has been paid to their mechanical properties. The mechanics of ternary TMDs, however, is of importance for the structural integrity and proper functioning of ternary TMD-based nanodevices. In particular, strain engineering is an efficient method to modify the electrical properties (e.g., the bandgap) of ternary TMDs.[30] Thus, a comprehensive understanding of the mechanical properties and behaviors of ternary TMDs plays a crucial role in the successful applications of ternary TMDs in different fields in the future.

In the present work, taking the recently synthesized monolayer $MoS_{2x}Te_{2(1-x)}$[22] as an example, the mechanical behaviors of ternary TMDs at finite temperatures have been investigated by tensile tests through molecular dynamics (MD) simulations. Efforts are made to examine the influence of the stoichiometric coefficient, temperature, and loading condition on Young's modulus and fracture behaviors of monolayer $MoS_{2x}Te_{2(1-x)}$. In addition, in terms of their mechanical properties, a comparative study is also conducted between the present alloyed $MoS_{2x}Te_{2(1-x)}$ nanosheets and their pristine counterparts including MoS_2 and $MoTe_2$ nanosheets. This work is anticipated to provide helpful insights into the future applications of $MoS_{2x}Te_{2(1-x)}$ nanosheets and exploiting their mechanical properties.

II. SIMULATION METHODS

Since MoS_2 and $MoTe_2$ crystals have a similar atomic structure, in the present simulation, the ternary TMD $MoS_{2x}Te_{2(1-x)}$ structures were initially constructed based on the atomic structure of pure MoS_2 crystals. Here, the structure of an MoS_2 crystal was obtained from first-principles calculations, in which the bond length between neighboring Mo and S atoms was 2.382 Å and the bond angle was 80.581°.[29] Subsequently, as shown in Fig. 1, according to the required stoichiometric coefficient x, the initial atomic structure of $MoS_{2x}Te_{2(1-x)}$ can be obtained via randomly replacing some S atoms in the initially constructed MoS_2 structures by Te atoms. A wide range of stoichiometric coefficients, i.e., $x = 0$, 0.2, 0.4, 0.6, 0.8, and 1 were set in our MD simulations. In experiments, the values of the stoichiometric coefficient can be controlled by environmental parameters depending on different synthesis methods. For example, through physical vapor deposition, the composition of Te in $MoTe_{2x}Se2_{(1-x)}$ alloys can be easily tailored by modifying the heating temperature of Te powders.

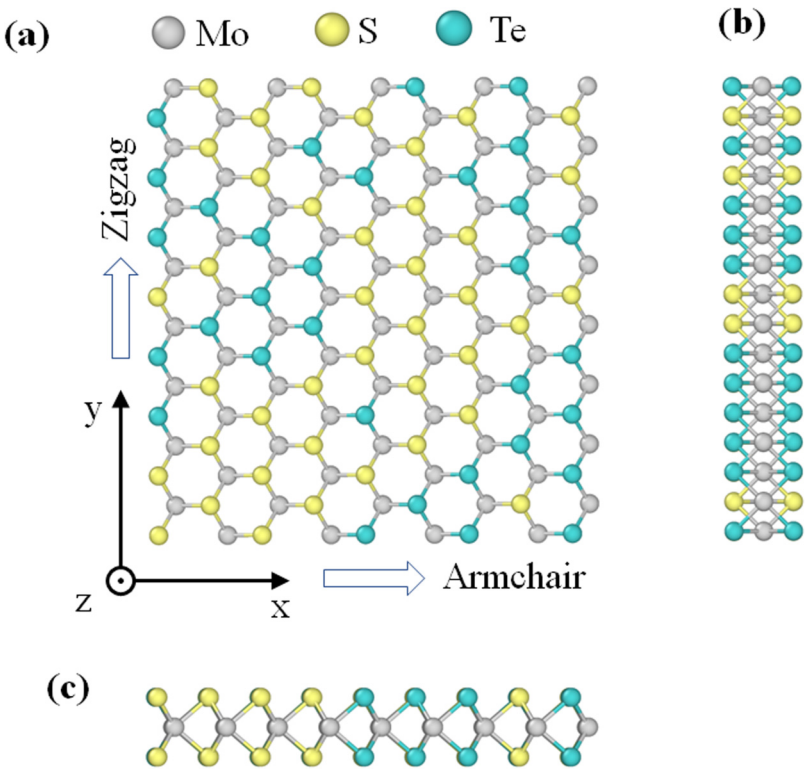

FIG. 1. (a) Top view of monolayer $MoS_{2x}Te_{2(1-x)}$. The different atom types are denoted by different colors. The armchair boundary is along the x direction, while the zigzag boundary is along the y direction. (b) Front view of monolayer $MoS_{2x}Te_{2(1-x)}$ in the y direction. (c) Side view of monolayer $MoS_{2x}Te_{2(1-x)}$ in the x direction.

Three stoichiometric coefficients $x = 0.07$, 0.165, and 0.32 of $MoTe_{2x}Se2_{(1-x)}$ were obtained in experiments.[43] The $MoS_{2x}Se_{2(1-x)}$ component can be precisely controlled by controlling the volatilization temperature of $MoSe_2$ and MoS_2.[44] By using chemical vapor deposition, the variation of the composition of $MoS_{2x}Se_{2(1-x)}$ alloy monolayers is found to depend on the proportion of volatilization of S/Se in the reaction. Seven stoichiometric coefficients x varying from 0 to 1 were obtained for the $MoS_{2x}Se_{2(1-x)}$ alloy monolayers.[26] Therefore, following the existing reports on other ternary TMDs, in the present work, we set a wide range of the stoichiometric coefficient x (0, 0.2, 0.4, 0.6, 0.8, and 1) of ternary $MoS_{2x}Te_{2(1-x)}$ to conduct a comprehensive study on the influence of the stoichiometric coefficient on the mechanical properties of this novel 2D material. The initial size of the $MoS_{2x}Te_{2(1-x)}$ structures constructed in our MD simulation is 100×100 Å^2. To investigate the mechanical properties of $MoS_{2x}Te_{2(1-x)}$ nanosheets, external loading was applied in their armchair and zigzag directions, which are, respectively, along the x and y axes (see Fig. 1).

The whole MD simulation process conducted in the present study was implemented by using the open-source simulation code LAMMPS,[30] in which the standard Newton equations of motion were integrated in time using the velocity Verlet algorithm with a time step of 1 fs. The periodic boundary conditions were applied along the in-plane x and y directions and the z direction (the thickness direction of the nanosheets). The size of the simulation box was set as $10 \times 10 \times 10$ nm^3. The periodic boundary in both in-plane directions was applied at the edges of nanosheets, while a vacuum space of 50 Å in the z direction was placed above and below the nanosheets to avoid interaction between adjacent layers. By applying the periodic boundary conditions[38] along both the armchair and zigzag directions, the 2D nanosheets can be replicated throughout the plane to form an infinite lattice. Thus, compared to the fixed boundary condition, the periodic boundary condition can effectively avoid the boundary effect of the system and thus make the calculation results more realistic. Actually, the periodic boundary conditions were widely used in MD simulations to calculate the mechanical properties of various nanomaterials such as the bulk graphene-based carbon foams,[39] MoS_2,[40,41] and phosphorene[42] nanosheets. The force interactions between atoms in our system were described by the Stillinger-Weber (SW) potential with parameters proposed by Jiang *et al.*[19,31,32] The potential parameters were achieved by fitting the SW potential to an experimentally obtained phonon spectrum. It is shown that the obtained empirical potential provides a good description of the energy gap and the crossover in the phonon spectrum.[20] Moreover, this potential has been successfully applied in studying the mechanical properties of MoS_2[33] and strain distribution in Mo-S-Te heterostructures, which are consistent with the experimental results.[32] Very recently, this potential also has been successfully used to calculate the mechanical and thermal properties of the MoS_2-WSe_2 lateral heterostructures.[36]

In the present study, the mechanical behaviors of monolayer $MoS_{2x}Te_{2(1-x)}$ nanosheets were investigated through the tensile test, which is an experimental method widely employed to characterize the mechanical properties of the materials. Since the correct molecular structure is of great importance in obtaining reliable results in MD simulations, the energy minimization and the structural relaxation should be performed before applying the tensile deformation on $MoS_{2x}Te_{2(1-x)}$ nanosheets. Here, the energy minimization was performed by the conjugate gradient method. Afterward, the system was relaxed at different temperatures, i.e., 100 K, 200 K, 300 K, 400 K, and 500 K, in an NPT ensemble (constant atom number, pressure, and temperature). During the structural relaxation process, in order to release all internal stresses, the hydrostatic pressure was set as zero. After a structural relaxation within 500 000 time steps, the equilibrium structure of $MoS_{2x}Te_{2(1-x)}$ nanosheets with stable energy, stable configuration, and zero internal stress was obtained. Figure 2 shows the size of different $MoS_{2x}Te_{2(1-x)}$ nanosheets with x ranging from 0 to 1. Here, as shown in Fig. 2(a), the length l_x, the width l_y, and the thickness l_z denote the size of $MoS_{2x}Te_{2(1-x)}$ nanosheets along their x, y, and z axes, respectively. It can be found from Figs. 2(b)–2(d) that l_x, l_y, and l_z of $MoS_{2x}Te_{2(1-x)}$ nanosheets under different temperatures (varying from 100 K to 500 K) are close to each other, which means that the structural size of $MoS_{2x}Te_{2(1-x)}$ nanosheets is less affected by the temperature. In the previous studies, the thermal expansion coefficient of the free-standing monolayer MoS_2 was reported to be $6.49 \pm 0.75 \times 10^{-5}$ K^{-1} obtained by combing experimental measurements and first-principles calculations.[37] As shown in Fig. S1(b) in the supplementary material, the thermal expansion coefficient of the present monolayer ternary TMD $MoS_{2x}Te_{2(1-x)}$ varies from 1.17×10^{-5} K^{-1} to 2.55×10^{-5} K^{-1}, which depends on their stoichiometric coefficient and is in the same order of magnitude as that of its MoS_2 counterpart. Under this small thermal expansion coefficient, the volume change of the present ternary TMD $MoS_{2x}Te_{2(1-x)}$ can be ignored, since the temperature in the present study only varies from 100 K to 500 K. Moreover, from Fig. 2, we can also see that the sizes in all directions (length, width, and thickness) of the nanosheets vary linearly with the increasing coefficient x. This phenomenon indicates that the structural sizes of $MoS_{2x}Te_{2(1-x)}$ nanosheets at different temperatures obey the same mixing rule, which can be written as

$$l_{MoS_{2x}Te_{2(1-x)}} = x l_{MoS_2} + (1-x) l_{MoTe_2} \quad (1)$$

where $l_{MoS_{2x}Te_{2(1-x)}}$, l_{MoS_2}, and l_{MoTe_2} represent the structural size of $MoS_{2x}Te_{2(1-x)}$, MoS_2, and $MoTe_2$ nanosheets, respectively.

After the energy minimization and structural relaxation processes, the uniaxial and biaxial loadings were applied to monolayer $MoS_{2x}Te_{2(1-x)}$ nanosheets, which make the structures elongated in the armchair direction, zigzag direction, and both directions. In this loading process, a very low strain rate of 0.0001 ps^{-1} was employed, which can effectively avoid the crystalline defects normally produced due to the high rate of loading.[33] In the simulation, the deformation was applied to the atoms by remapping the atom positions each time after the simulation box size was changed. All tensile tests were performed in the NPT ensemble (constant atom number, pressure, and temperature). Specifically, the pressure along the lateral direction that was perpendicular to the stretching direction of nanosheets was set to zero in response to the tensile strain dynamically. Here, the engineering strain ε was defined as $\varepsilon = (L - L_0)/L_0$, where L and L_0 are the lengths of $MoS_{2x}Te_{2(1-x)}$ nanosheets after and before the deformation, respectively. Meanwhile, the stress σ was calculated using the virial stress

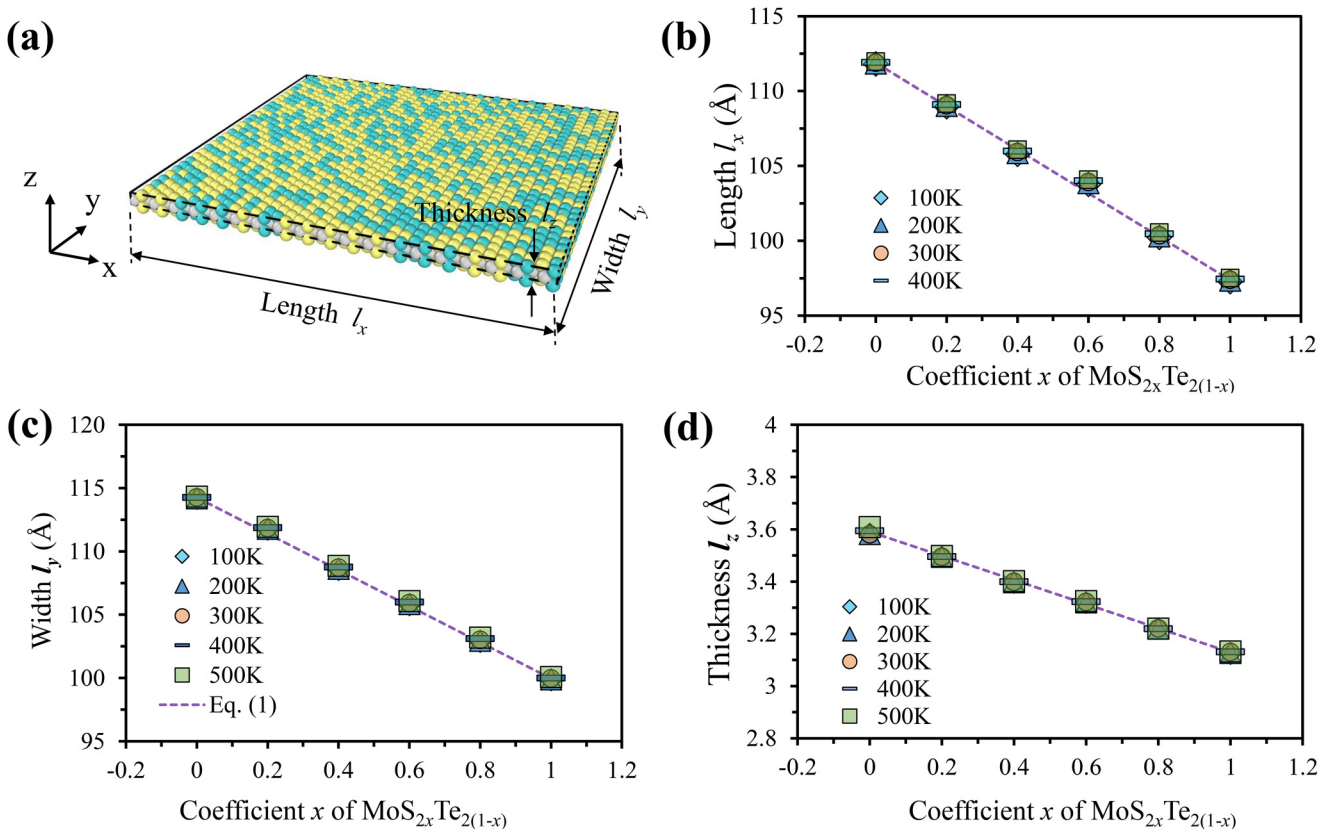

FIG. 2. (a) Schematic plot to illustrate the size of monolayer $MoS_{2x}Te_{2(1-x)}$. The dimensions along x, y, and z directions are length l_x, width l_y, and thickness l_z, respectively. The length and width are calculated as the average size of the system in x and y axes, respectively. The thickness is calculated as the average distance between atoms in top and bottom layers. (b) Length l_x, (c) width l_y, and (d) thickness l_z of monolayer $MoS_{2x}Te_{2(1-x)}$ with different coefficients x and at different temperatures after energy minimization and structural relaxation.

formulation, which is taken as the arithmetic mean of the local stresses on all atoms and has the following expression:[34,35]

$$\sigma = \frac{1}{V}\sum_{i=1}^{N}\left(m_i v_a^i v_a^i + \frac{1}{2}\sum_{j\neq i}^{N} F_a^{ij} r_a^{ij}\right), \tag{2}$$

where V and N are the volume and total atom number of the system; m_i and $vi\ a$ denote the mass and axial velocity of atom i; F_a^{ij} and r_a^{ij} represent the force and distance between atoms i and j. Note that the Einstein summation convention for indicator a was used in Eq. (2). Here, the volume of the $MoS_{2x}Te_{2(1-x)}$ nanosheet system was calculated from

$$V = l_x l_y l_z. \tag{3}$$

It is worth noting that the thickness of monolayer $MoS_{2x}Te_{2(1-x)}$ nanosheets was taken as the average distance between atoms located at the top and bottom layers.[32]

III. RESULTS AND DISCUSSION

In this section, MD simulation-based tensile tests were employed to study the mechanical behaviors of $MoS_{2x}Te_{2(1-x)}$ nanosheets under two loading conditions: the uniaxial tension along armchair and zigzag directions and the biaxial tension along both directions. The influence of the stoichiometric coefficient on the fracture properties and elastic properties of $MoS_{2x}Te_{2(1-x)}$ nanosheets was quantified. It should be noted that ternary $MoS_{2x}Te_{2(1-x)}$ nanosheets of different random distributions were built to evaluate the dispersion of the mechanical properties of these alloyed TMD monolayers. Taking $MoS_{0.4}Te_{1.6}$ as an example, its mechanical properties (Young's modulus and ultimate strength) with eight different random distributions are shown in Fig. S2 in the supplementary material. Here, the tensile tests were performed along the armchair direction by setting the system temperature as 300 K. It is shown in Fig. S2 in the supplementary material that Young's modulus and ultimate strength of the alloyed TMD monolayers both trivially depend on the distribution of the alloying element. Under this circumstance,

to simplify our analysis without losing generality, one sample of each $MoS_{2x}Te_{2(1-x)}$ was taken as a representative example in the present study.

A. Uniaxial tension

1. Uniaxial tension along the armchair direction

The tensile test was first conducted to $MoS_{2x}Te_{2(1-x)}$ nanosheets by uniaxially stretching them along their armchair direction. The stress-strain curves of $MoS_{2x}Te_{2(1-x)}$ nanosheets at five different temperatures (T = 100 K, 200 K, 300 K, 400 K, and 500 K) are plotted in Fig. 3. Comparing the stress-strain curves of the alloyed TMD monolayers, i.e., $MoS_{2x}Te_{2(1-x)}$ $(0.2 \le x \le 0.8)$ to those of their pristine TMD counterparts, i.e., MoS_2 and $MoTe_2$, we can see that the pristine and alloyed TMD monolayers exhibit different fracture modes. Specifically, the fracture mode of the pristine MoS_2 and $MoTe_2$ nanosheets are in a brittle fracture manner, since these materials completely break with a sudden drop of the

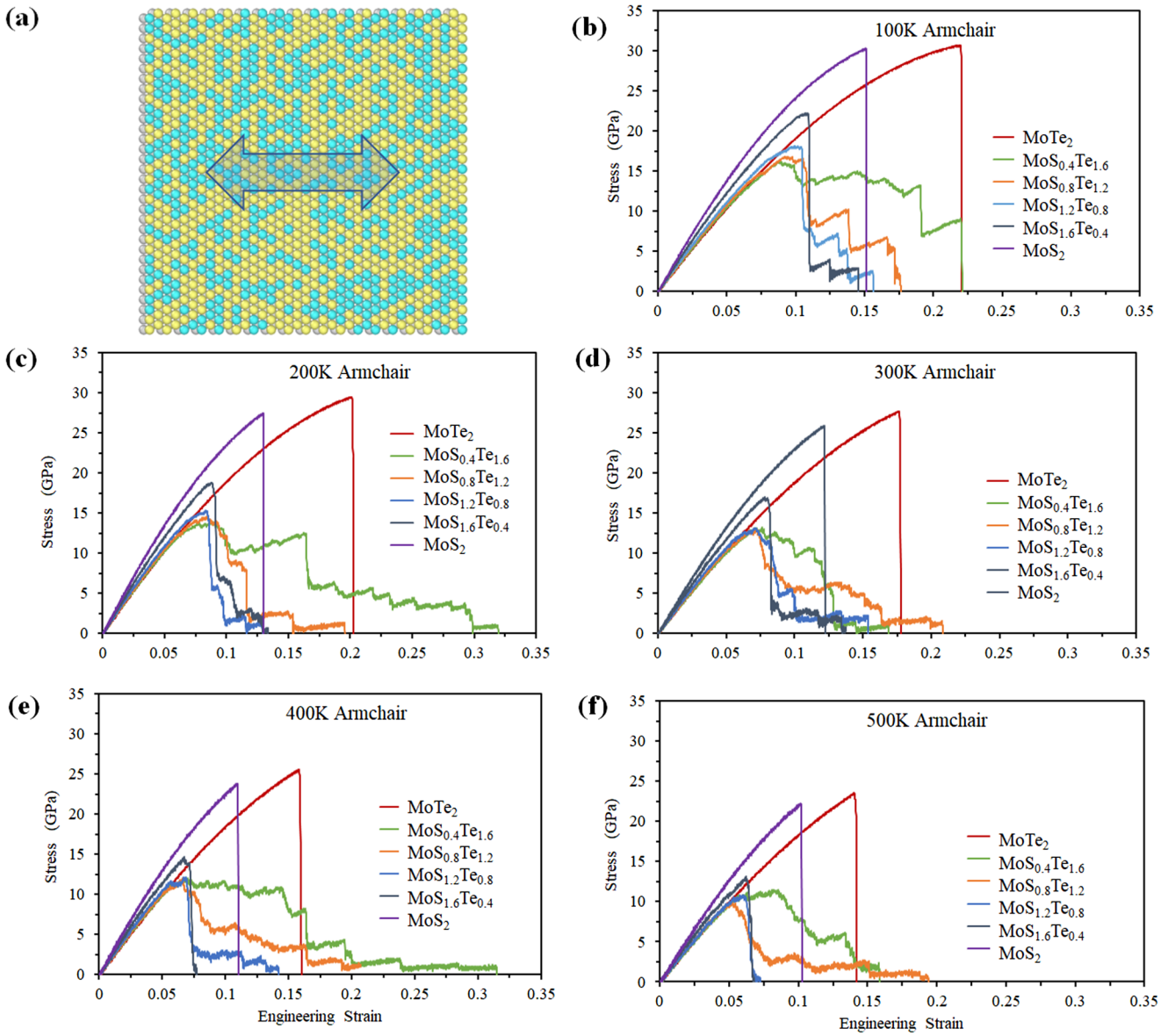

FIG. 3. (a) Diagram of the tensile test simulation of monolayer $MoS_{2x}Te_{2(1-x)}$ stretched along the armchair direction. (b)–(f) Stress-strain curves of monolayer $MoS_{2x}Te_{2(1-x)}$ under 100 K, 200 K, 300 K, 400 K, and 500 K, respectively.

stress from its maximum value to zero, which corresponds to the physical process from the nucleation of initial voids to the final rupture. However, the alloyed monolayer ternary TMDs exhibit a ductile fracture behavior after their stress reaches the ultimate strength, since their stress-strain curves are found to have many descending steps until the final failure. At some specific temperatures, such as 200 K and 400 K, the fracture strain of $MoS_{0.4}Te_{1.6}$ can reach up to 0.32, which is much larger than the value of other alloyed $MoS_{2x}Te_{2(1-x)}$, the pristine MoS_2 and $MoTe_2$, nanosheets. Based on these findings, we can come to the conclusion that the alloyed $MoS_{2x}Te_{2(1-x)}$ nanosheets, specifically those with a stoichiometric coefficient of 0.2, possess a relatively strong toughness.

In Figs. 4(a) and 4(b), taking MoS_2 at 100 K and $MoS_{0.4}Te_{1.6}$ at 200 K as typical examples, we show the evolution of the brittle fracture in pristine monolayer TMDs and the ductile fracture in their alloyed counterparts. It is found that at $\varepsilon < 0.1511$, no voids are observed in MoS_2 nanosheets. However, the initial void nucleates at $\varepsilon = 0.1512$, which leads to the sudden rupture of the entire MoS_2 nanosheets at $\varepsilon = 0.1518$. From the crack initiation at $\varepsilon = 0.1512$ to the complete fracture at $\varepsilon = 0.1516$, the entire fracture process of MoS_2 nanosheets in our MD simulations lasts 4 ps. However, as for the alloyed $MoS_{0.4}Te_{1.6}$ nanosheets, the initial voids can be observed at a relatively small strain of $\varepsilon = 0.09$. Afterward, with increasing the tensile strain from 0.09 to 0.1, the voids further expand and gradually aggregate into several line defects. Subsequently, these line defects overcome the resistance of some bonds nearby the existing cracks, resulting in the occurrence of a whole line defect. If we keep increasing the strain to $\varepsilon = 0.17$, the entire line defect widens with the continuously growing tensile strain and finally evolves into a surface defect inside the $MoS_{0.4}Te_{1.6}$ nanosheets. When the strain further grows to 0.25, the increase of the surface defect inside monolayer $MoS_{0.4}Te_{1.6}$ causes the separation of the entire nanosheet into two parts connected by three bridging atomic chains. These two bridging atomic chains break at $\varepsilon = 0.30$ and 0.3194, respectively. The breakage of the last atomic chain indicates the complete fracture of the nanosheet at the fracture strain $\varepsilon = 0.32$. During the fracture process, the strains corresponding to the crack initiation and the complete fracture of $MoS_{0.4}Te_{1.6}$ nanosheets are, respectively, 0.09 and 0.32, which means that the entire fracture process in alloyed $MoS_{0.4}Te_{1.6}$

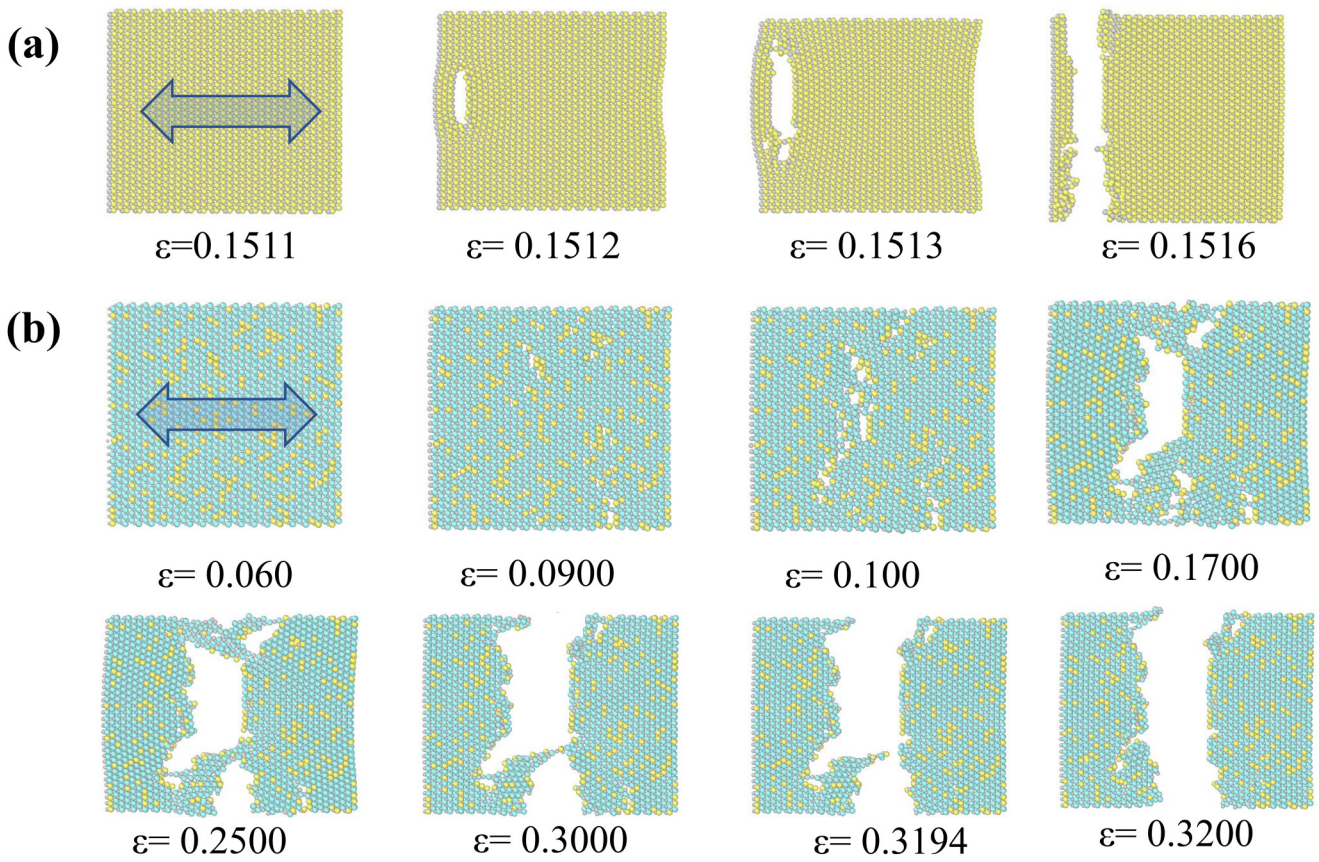

FIG. 4. Two different fracture modes occurring in pristine and alloyed monolayer TMDs during tensile loading along the armchair direction. (a) Brittle fracture in MoS_2 nanosheets at 100 K. (b) Ductile fracture in $MoS_{0.4}Te_{1.6}$ nanosheets at 200 K.

nanosheets can last 2300 ps in our MD simulations. The duration of the ductile fracture in the alloyed $MoS_{0.4}Te_{1.6}$ nanosheets is 575 times that of the pristine MoS_2 nanosheets, which is the most significant difference between two fracture modes observed in alloyed and pristine monolayer TMDs. It is worth mentioning that, in Fig. 4(a), the void initiates from the interior of the nanosheets rather than their edges, because the boundary effect is excluded in the present simulation with periodic boundaries, which, compared to the simulations with the nonperiodic boundary, is more accurate in calculating the mechanical properties of a bulk 2D material.[33,42]

Young's modulus and ultimate strength extracted from stress-strain curves of monolayer $MoS_{2x}Te_{2(1-x)}$ with different stoichiometric coefficients are plotted in Figs. 5(a) and 5(b), respectively. Young's modulus E was obtained through $E = \Delta\sigma/\Delta\varepsilon$, where $\Delta\varepsilon$ is the increment in the strain and $\Delta\sigma$ is the corresponding increment in the stress. It is noted that to maintain the assumption of linear elasticity, Young's modulus was calculated by fitting the stress against strain under $\varepsilon < 0.03$. The ultimate strength was calculated as the largest stress sustained by monolayer $MoS_{2x}Te_{2(1-x)}$ during the entire tensile process. As shown in Fig. 5(a), when the system temperature is set as 100 K, Young's modulus of monolayer $MoS_{2x}Te_{2(1-x)}$ keeps almost unchanged when the stoichiometric coefficient varies in the range of 0–0.4. However, Young's modulus increases apparently when the stoichiometric coefficient increases from 0.6 to 1. In general, a nonlinear relationship between Young's modulus and the stoichiometric coefficient is observed, which shows a parabola shape, as illustrated in Fig. 5(a). A similar relationship between Young's modulus and the stoichiometric coefficient is observed in monolayer $MoS_{2x}Te_{2(1-x)}$ at 200 K, 300 K, 400 K, and 500 K.

Figure 5(a) shows that Young's moduli of monolayer $MoTe_2$, $MoS_{0.4}Te_{1.6}$, and $MoS_{0.8}Te_{1.2}$ (i.e., $x = 0$, 0.2, and 0.4) are extremely close to each other, which denotes that Young's modulus of the $MoTe_2$ nanosheet is insensitive to the number of the doping S atoms in the binary nanosheet. Conversely, Young's moduli of monolayer MoS_2, $MoS_{1.6}Te_{0.4}$, and $MoS_{1.2}Te_{0.8}$ (i.e., $x = 1$, 0.8, and 0.6) decrease rapidly as x decreases, indicating that Young's modulus of the MoS_2 nanosheet is very sensitive to the number of the doping Te atoms in the binary nanosheet. Figure 5(b) shows the ultimate strength of monolayer $MoS_{2x}Te_{2(1-x)}$ with different stoichiometric coefficients when they are under tensile loading in the armchair direction. It is shown in Fig. 5(b) that, with increasing the stoichiometric coefficient from 0 to 1, the ultimate strength of monolayer $MoS_{2x}Te_{2(1-x)}$ at different temperatures first decreases and then increases. In other words, the pristine binary $MoTe_2$ ($x = 0$) and MoS_2 ($x = 1$) possess a relatively large ultimate strength,

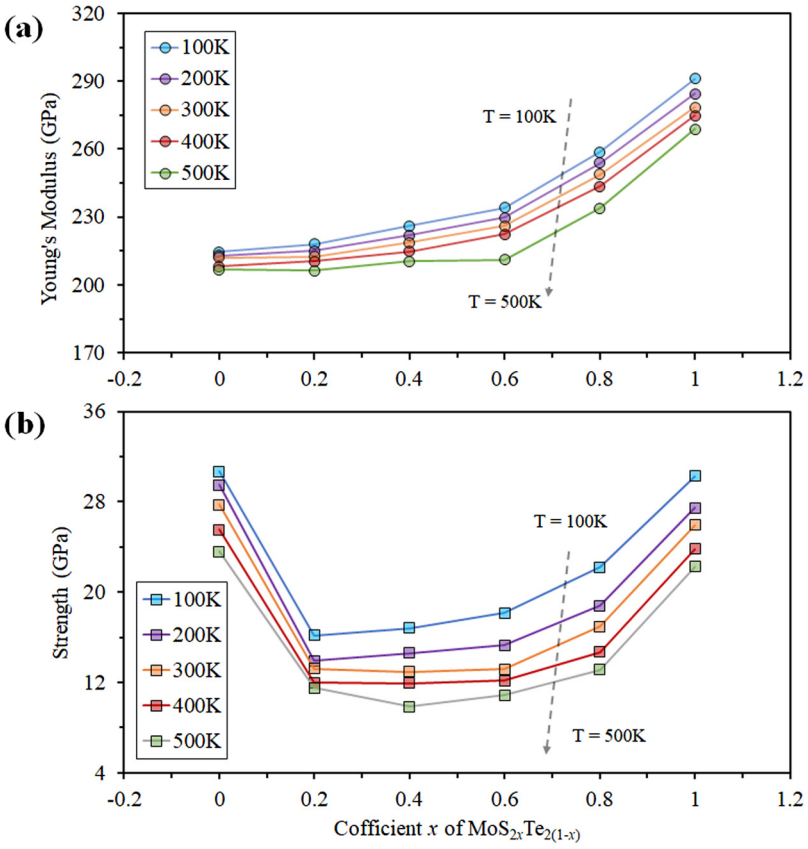

FIG. 5. (a) Young's modulus and (b) ultimate strength of $MoS_{2x}Te_{2(1-x)}$ nanosheets with different stoichiometric coefficients x when they are under tensile loading along the armchair direction. Five different temperatures in the range of 100 K–500 K are considered.

while the alloyed ternary TMDs such as $MoS_{0.4}Te_{1.6}$, $MoS_{0.8}Te_{1.2}$, $MoS_{1.2}Te_{0.8}$, and $MoS_{1.6}Te_{0.4}$ have a relatively small ultimate strength. Moreover, the temperatures are also found to have a significant effect on the ultimate strength of monolayer TMDs. For example, when the temperatures are 100 K and 200 K, the smallest ultimate strength is found in the $MoS_{0.4}Te_{1.6}$ nanosheets. However, the $MoS_{1.2}Te_{0.8}$ nanosheets are found to possess the smallest ultimate strength when the temperatures are 300 K, 400 K, and 500 K. From the above results, we can conclude that the ultimate strength of the pristine binary TMD nanosheets is generally much larger than that of their alloyed ternary TMD counterparts. This phenomenon is mainly attributed to the uncoordinated deformation in the alloyed ternary TMDs ($MoS_{2x}Te_{2(1-x)}$) caused by the stress concentration between Te atoms and their nearby S atoms, which makes voids that may occur at a relatively small strain, i.e., $\varepsilon < 0.1$ [see Figs. 3(b)–(f)]. The initial cracks thus begin to gradually expand in the alloyed ternary TMDs under further tensile loading. However, in the undoped binary structures (i.e., pristine monolayer TMDs), the stress reaches the maximum value and immediately declines to zero at a relatively large strain.

In addition, comparing Young's modulus and ultimate strength of monolayer $MoS_{2x}Te_{2(1-x)}$ at five different temperatures illustrated in Figs. 5(a) and 5(b), we can see that the values at a relatively low temperature are larger than those at a relatively high temperature. This finding indicates that both Young's modulus and ultimate strength of TMD nanosheets decrease as the temperature increases. This temperature-induced softening is mainly caused by the increasing amplitude of thermal vibrations of atoms at a relatively high temperature, which makes the chemical bonds easier to reach the cutoff radius and, therefore, break. In order to provide a quantitative description of the temperature-induced softening phenomenon, in Fig. 6, we graphically show Young's modulus and ultimate strength of ternary TMDs as a function of the temperature varying from 100 K to 500 K. Generally, these material parameters reduce significantly with increasing temperature. For instance, when the temperature increases from 100 K to 500 K, Young's modulus of $MoS_{1.6}Te_{0.4}$ in the armchair direction reduces by 9.6%. In the same process, the ultimate strength reduces by 40.9%. Furthermore, as shown in Fig. 6, both Young's modulus and ultimate strength show a linear relationship with the temperature. The relationship between Young's modulus (ultimate strength) and the

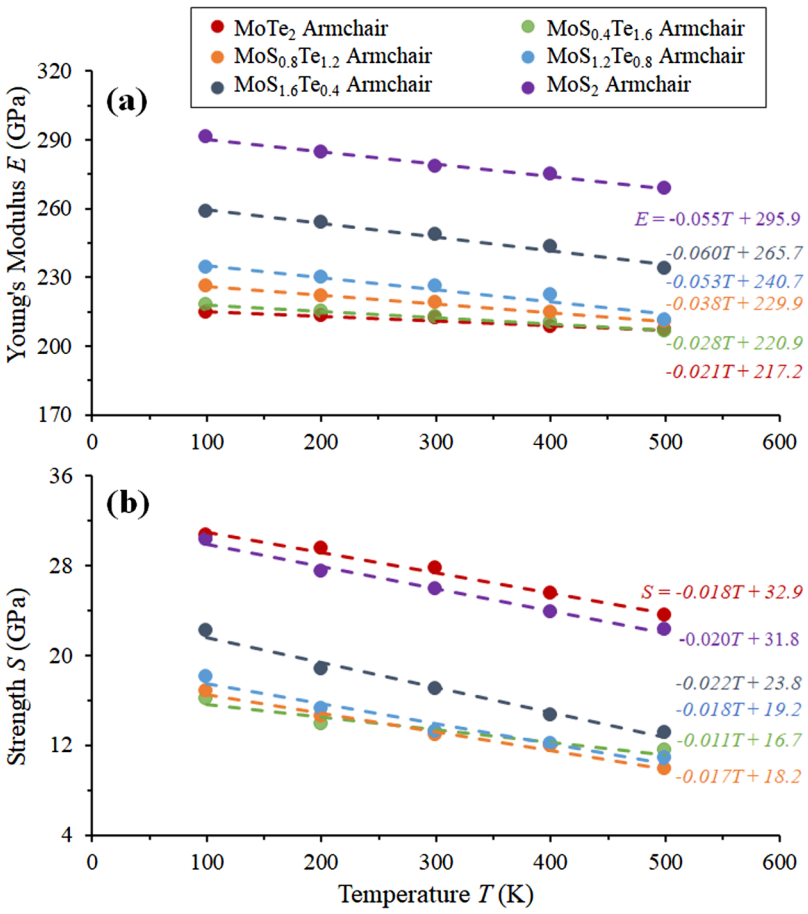

FIG. 6. (a) Young's modulus E and (b) ultimate strength S of ternary $MoS_{2x}Te_{2(1-x)}$ nanosheets under different temperatures when they are under tensile loading along the armchair direction.

temperature can be expressed as

$$E(\text{or } S) = E_0(\text{or } S_0) - \alpha(\text{or } \beta)T. \quad (4)$$

Here, E and S are Young's modulus and the ultimate strength of the nanosheets at temperature T, respectively. E_0 and S_0 are Young's modulus and the ultimate strength of the nanosheets at 0 K. α and β are temperature dependence coefficients that need to be determined. Values of E_0, S_0, α, and β can be obtained by applying a linear fitting to the data shown in Fig. 6. As shown in Fig. 6, both E_0 and α of $MoS_{2x}Te_{2(1-x)}$ increases monotonically with increasing stoichiometric coefficient x, which means that the MoS_2 nanosheet has a larger Young's modulus and a stronger temperature-induced softening effect than the $MoTe_2$

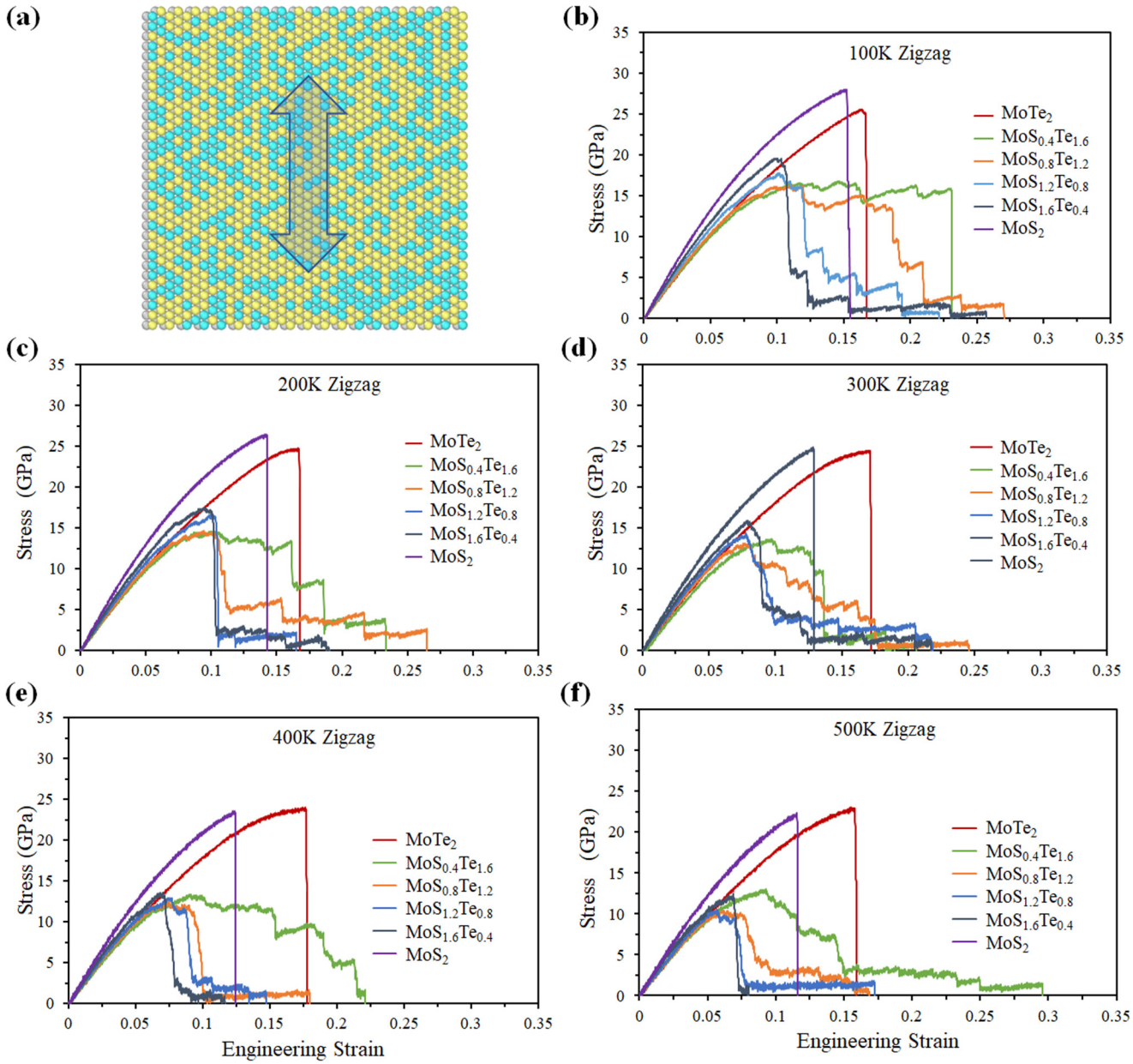

FIG. 7. (a) Diagram of the tensile test simulation of monolayer $MoS_{2x}Te_{2(1-x)}$ stretched along the zigzag direction. (b)–(f) Stress-strain curves of monolayer $MoS_{2x}Te_{2(1-x)}$ under 100 K, 200 K, 300 K, 400 K, and 500 K, respectively.

nanosheet. Moreover, Young's modulus and temperature-induced softening effect can be effectively tuned by the stoichiometric coefficient x. As for the ultimate strength, its temperature dependence coefficient β varies between 0.011 and 0.022, which is generally smaller than the coefficient α of Young's modulus varying from 0.021 to 0.06. All TMDs show a significant loss in strength with increasing temperature, which should be highly taken into account in future applications of alloyed ternary TMDs, specifically in tuning their bandgap through the strain engineering.

2. Uniaxial tension along the zigzag direction

Next, as illustrated in Fig. 7(a), monolayer $MoS_{2x}Te_{2(1-x)}$ nanosheets were stretched along the zigzag direction that is perpendicular to the armchair direction with the same strain rate of 0.0001 ps^{-1} as we employed above. The stress-strain curves obtained from the tensile test simulation at five different temperatures are plotted in Figs. 7(b)–7(f). It is apparent that two distinctly different fracture modes are found in pristine monolayer TMDs and alloyed monolayer TMDs, which is similar to the result extracted from the same nanosheets under the tension along the armchair direction. Specifically, a brittle fracture is found in two pristine binary TMDs (MoS_2 and $MoTe_2$), while a ductile fracture is detected in alloyed ternary TMDs ($MoS_{0.4}Te_{1.6}$, $MoS_{0.8}Te_{1.2}$, $MoS_{1.2}Te_{0.8}$, and $MoS_{1.6}Te_{0.4}$). The fracture strain of the alloyed ternary TMDs is much larger than that of their pristine binary TMD counterparts. Moreover, the fracture strain of the ternary TMDs stretched along the zigzag direction is much larger than that of their counterparts stretched along the armchair direction (see Fig. 3), which indicates that the ternary TMDs have larger flexibility in the zigzag direction. To better show the different fracture behaviors observed in pristine and alloyed TMD nanosheets, taking MoS_2 nanosheets at 300 K and $MoS_{0.4}Te_{1.6}$ nanosheets at 500 K as examples, in Fig. 8, we show their atomic structures during the fracture process extracted from MD simulations. In Fig. 8(a), the entire fracture process of MoS_2 nanosheets under a temperature of 300 K finishes quickly within an extremely short time of 10 ps, during which the initial voids are generated at $\varepsilon = 0.129$ and the final fracture occurs at

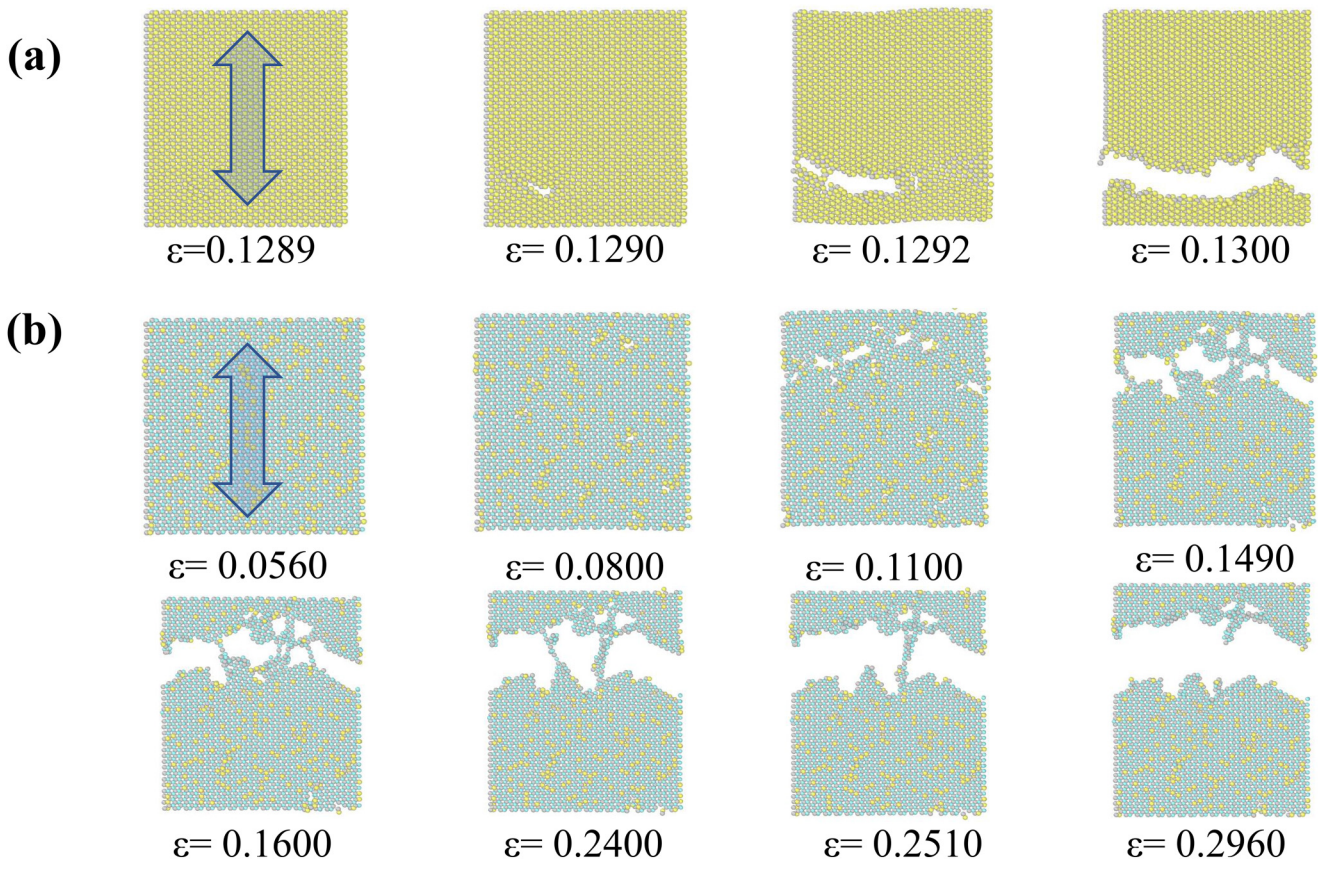

FIG. 8. Two different fracture modes occurring in pristine and alloyed monolayer TMDs during tensile loading along the zigzag direction. (a) Brittle fracture in MoS_2 nanosheets at 300 K. (b) Ductile fracture in $MoS_{0.4}Te_{1.6}$ nanosheets at 500 K.

$\varepsilon = 0.13$. Conversely, in Fig. 8(b), we find that the entire fracture process of $MoS_{0.4}Te_{1.6}$ nanosheets at 300 K endures a much longer time (2160 ps). During the fracture of monolayer $MoS_{0.4}Te_{1.6}$, the initial voids firstly occur at $\varepsilon = 0.08$, which expand into linear defects at $\varepsilon = 0.11$. These linear defect cracks further evolve into surface defects at $\varepsilon = 0.149$, which induces several bridging atomic chains occurring in the materials. These atomic chains gradually break at the strain between 0.24 and 0.251, resulting in the complete fracture of the nanosheets at the ultimate strain of 0.296. Due to different fracture modes observed in pristine and alloyed TMD nanosheets, the ductile fracture duration of the alloyed TMD nanosheets is 215 times larger than that of their pristine counterparts possessing the brittle fracture.

Figures 9(a) and 9(b) show Young's modulus and ultimate strength of monolayer $MoS_{2x}Te_{2(1-x)}$ nanosheets with different stoichiometric coefficients when they are under tensile loading along the zigzag direction, respectively. The overall changing trend of both Young's modulus and ultimate strength in the zigzag direction of monolayer $MoS_{2x}Te_{2(1-x)}$ with varied stoichiometric coefficients is close to the result in the armchair direction. Specifically, Young's modulus is found to change trivially when the stoichiometric coefficient x varies in the range of 0–0.4, while a significant increase is found when x grows from 0.4 to 1. This finding is consistent with the result extracted from the monolayer $MoS_{2x}Te_{2(1-x)}$ stretched along the armchair direction, whose Young's modulus is almost independent with the stoichiometric coefficient at $0 \le x \le 0.4$ but is strongly sensitive to the change of the stoichiometric coefficient at $0.6 \le x \le 1$. As for the ultimate strength of monolayer TMDs with different stoichiometric coefficients, it is found from Fig. 9(b) that the pristine monolayer TMDs possess relatively large ultimate strength, while their alloyed counterparts have a relatively small value. This result is also consistent with the result extracted from the nanosheets under tensile loading along the armchair direction. In addition to the stoichiometric coefficient, Young's modulus and ultimate strength of TMD nanosheets are also found to be affected by the temperature. Similar to the results of TMD nanosheets stretched in the armchair direction, as shown in Fig. 10, Young's modulus and ultimate strength of TMD nanosheets stretched along the zigzag direction decrease with growing temperature and thus show a temperature-induced softening phenomenon. The dotted line in Fig. 10 was also obtained by fitting Eq. (4) to the MD results. Except for $MoS_{1.6}Te_{0.4}$ ($x = 0.8$) whose α is slightly smaller than that of

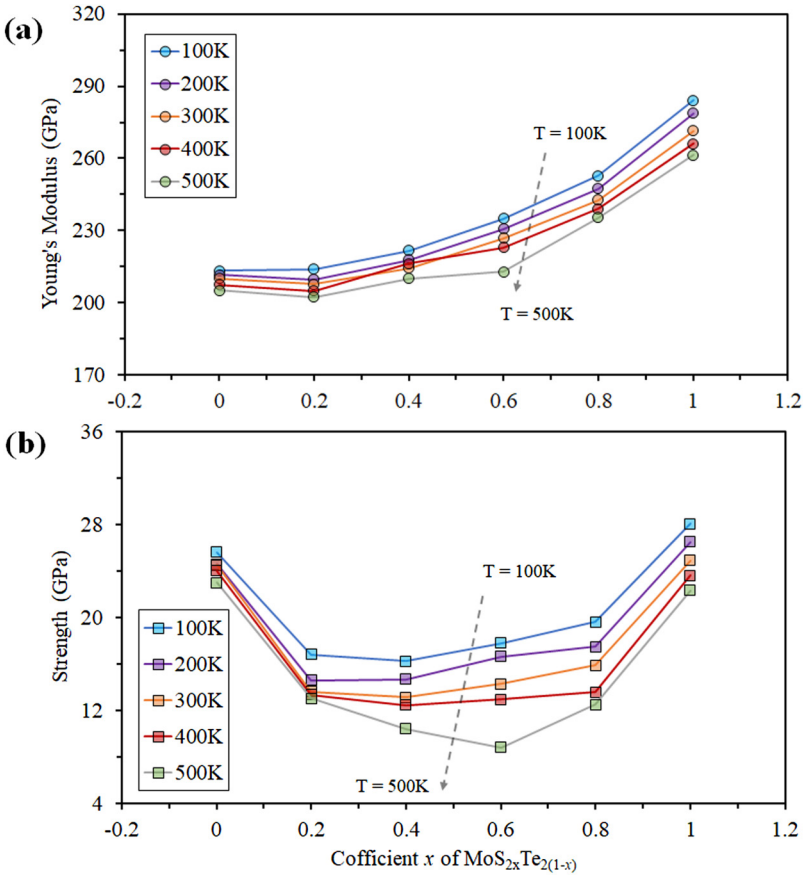

FIG. 9. (a) Young's modulus and (b) ultimate strength of $MoS_{2x}Te_{2(1-x)}$ nanosheets with different stoichiometric coefficients x when they are under tensile loading along the zigzag direction. Five different temperatures in the range of 100 K–500 K are considered.

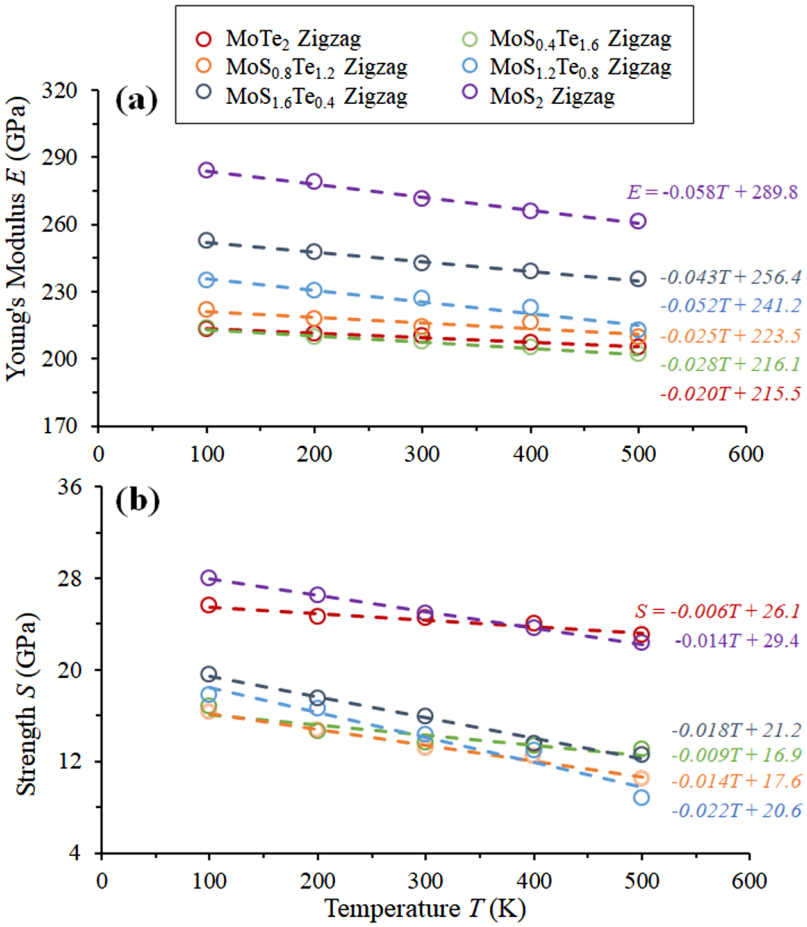

FIG. 10. (a) Young's modulus E and (b) ultimate strength S of ternary $MoS_{2x}Te_{2(1-x)}$ nanosheets under different temperatures when they are under tensile loading along the zigzag direction.

$MoS_{1.2}Te_{0.8}$ ($x = 0.6$), E_0 and α of other $MoS_{2x}Te_{2(1-x)}$ stretched along the zigzag direction increase generally with increasing coefficient x, which is similar to the result observed in its counterpart stretched along the armchair direction. Moreover, among all nanosheets considered here, Young's modulus of $MoS_{1.2}Te_{0.8}$ shows the largest dependence on the temperature, which is reduced by 9.39% when the temperature increases from 100 K to 500 K. In contrast, Young's modulus of $MoTe_2$ shows the smallest dependence on the temperature, which is reduced by only 3.79% when the temperature grows from 100 K to 500 K. As for the ultimate strength, the temperature dependence coefficient β of $MoS_{2x}Te_{2(1-x)}$ with x in the range of 0–0.4 is significantly smaller than the result of $MoS_{2x}Te_{2(1-x)}$ whose x is in the range of 0.6–1. This result is consistent with the result of the coefficient α. The above results indicate that, when the nanosheets are stretched along the zigzag direction, the mechanical properties of $MoTe_2$ are less dependent on the temperature than those of MoS_2.

In addition to Young's modulus and ultimate strength, Poisson's ratios under uniaxial tension in both armchair and zigzag directions were also calculated. Poisson's ratios of six TMD nanosheets under different temperatures ranging from 100 K to 500 K are plotted in Fig. S3 in the supplementary material. It is noted that Poisson's ratios obtained here were averaged by 100 results of nanosheets with a tensile strain in the range between 2.5% and 3.5% to mitigate the stress fluctuations induced by thermal fluctuations. The obtained Poisson's ratios are in the range of 0.2–0.4. Moreover, Poisson's ratio in the zigzag direction is generally greater than that in the armchair direction, which is consistent with the result of MoS_2 and $MoTe_2$ reported in the previous studies.[45–47]

B. Biaxial tension

The 2D materials are often under the biaxial loading in their practical applications. Therefore, it is necessary to know the mechanical behavior of monolayer $MoS_{2x}Te_{2(1-x)}$ under biaxial tension. Here, similar MD simulations were conducted to investigate the mechanical behavior of monolayer $MoS_{2x}Te_{2(1-x)}$ under biaxial tensile loading. As illustrated in Fig. 11(a), in the simulation process of the biaxial tension, the loading was applied along both the armchair and zigzag directions simultaneously at a strain rate

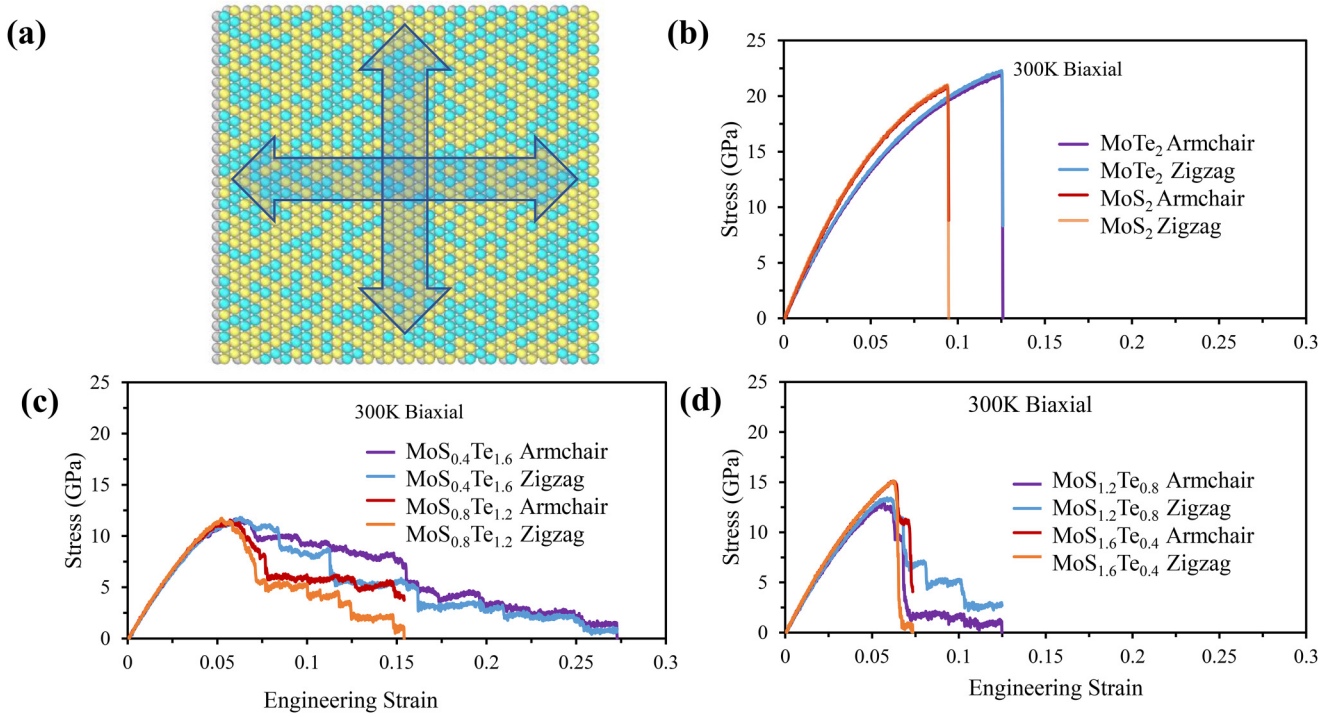

FIG. 11. (a) Diagram of the tensile test simulation of monolayer $MoS_{2x}Te_{2(1-x)}$ stretched biaxially at room temperature. (b) Stress-strain curves of monolayer MoS_2 and $MoTe_2$. (c) Stress-strain curves of monolayer $MoS_{0.4}Te_{1.6}$ and $MoS_{0.8}Te_{1.2}$. (d) Stress-strain curves of monolayer $MoS_{1.2}Te_{0.8}$ and $MoS_{1.6}Te_{0.4}$.

of 0.0001 ps^{-1}. Figures 11(b)–11(d) show the stress-strain curves of monolayer $MoS_{2x}Te_{2(1-x)}$ biaxially stretched under the room temperature (300 K). The pristine binary TMDs considered here, i.e., MoS_2 and $MoTe_2$ shown in Fig. 11(b), exhibit a brittle fracture behavior. Taking $MoTe_2$ as a typical example of binary TMDs, the structure evolution of $MoTe_2$ nanosheets under different biaxial deformations is plotted in Fig. 12(a). It is found that the initial voids occur when the tensile strain increases from 0.125 to 0.1254, which thus converge a surface defect. As the applied strain increases, the surface defect at the right edge keeps expanding along the 45° direction, which makes the resultant force in this region approach its maximum. Due to this effect, the complete fracture finally occurs in the nanosheets at an ultimate strain of 0.1271. To better show the fracture behaviors of alloyed ternary TMDs, in Fig. 12(b), we show the molecular structures of $MoS_{0.4}Te_{1.6}$ under biaxial tension during its fracture process. It is found that the entire ductile fracture process observed in the present nanosheets under biaxial loading is similar to that observed in their counterparts under the uniaxial loading along either the armchair [see Fig. 4(b)] or the zigzag direction [see Fig. 8(b)]. Specifically, during the entire fracture process, the initial voids, i.e., the dot defects, form at $\varepsilon = 0.06$, which thus aggregate into some line defects at $\varepsilon = 0.08$. Afterward, the line defects extend into the surface defects at $\varepsilon = 0.12$, the expansion of which triggers the gradual breaking of the bridging atomic chains at $\varepsilon = 0.17$–0.30. Finally, the complete fracture of the nanosheets happens at an ultimate strain of 0.325. After the final fracture, the fracture shapes of the nanosheets under biaxial loading are found to be different from those of their counterparts under uniaxial loading. As shown in Fig. S4 in the supplementary material, the cracks in the uniaxially loaded $MoS_{0.4}Te_{1.6}$ nanosheets are found to develop perpendicular to the loading direction, while the nanosheets under biaxial loading have a cross-shaped crack.

All alloyed ternary TMDs show obvious ductile fracture phenomena as illustrated in Figs. 11(c) and 11(d). The stress of monolayer $MoS_{2x}Te_{2(1-x)}$ increases linearly with the growing strain at the stage of strain ranging from 0 to 0.03, corresponding to the elastic deformation at this stage of strain. At this stage, the stress-strain curves of the nanosheets stretched along two directions coincide well with each other, which demonstrates that the monolayer $MoS_{2x}Te_{2(1-x)}$ exhibits the isotropic elastic behavior. Thus, the monolayer nanosheet can be regarded as a thin isotropic sheet under the small deformation condition. Under this circumstance, the effective modulus of monolayer $MoS_{2x}Te_{2(1-x)}$ under biaxial stretching $E_{biaxial}$ can be calculated from[48]

$$E_{biaxial} = E(1-\nu) = 0.5(E_{bi\text{-}armchair} + E_{bi\text{-}zigzag}) \times [1 - 0.5(\nu_{armchair} + \nu_{zigzag})], \quad (5)$$

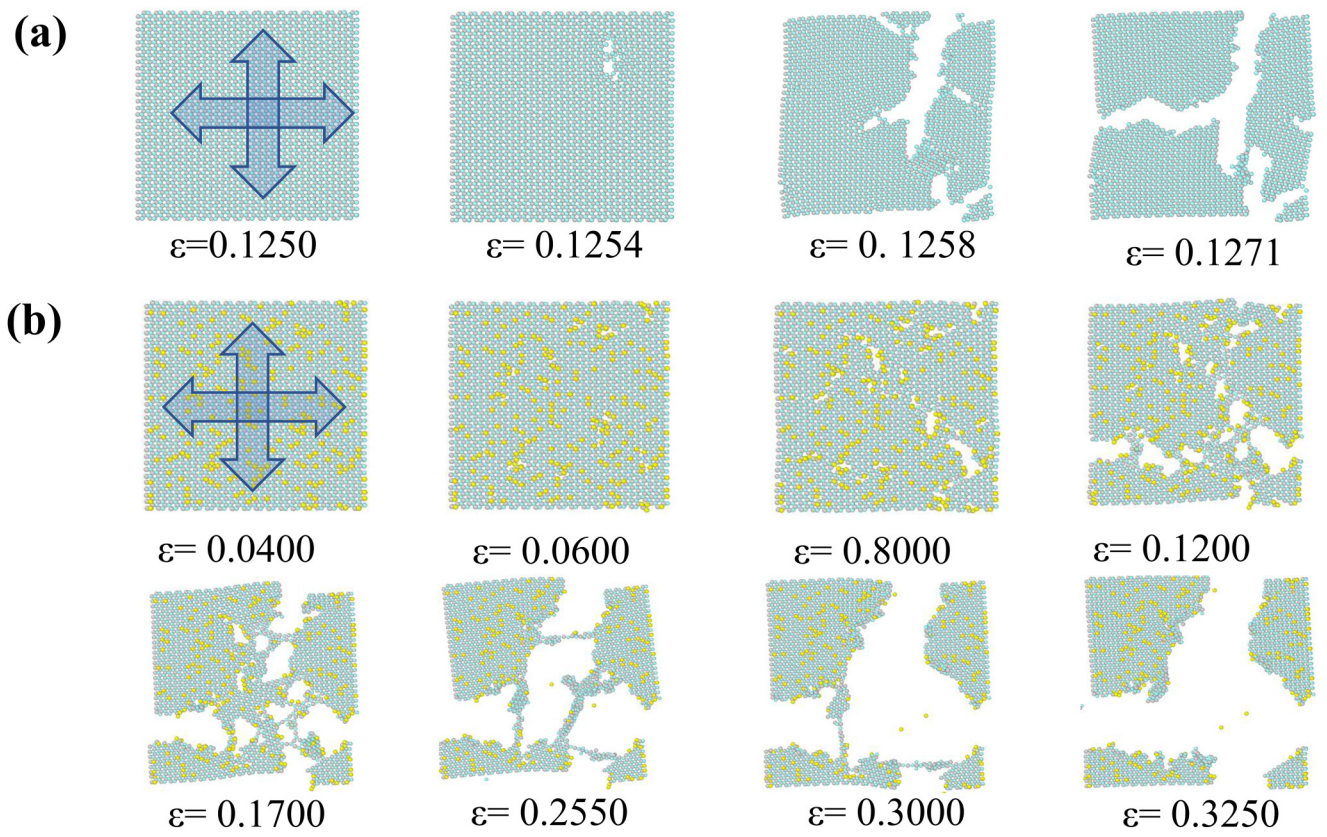

FIG. 12. Fracture process of (a) monolayer $MoTe_2$ and (b) monolayer $MoS_{0.4}Te_{1.6}$ under biaxial tensile loading. The system temperature is set as 300 K.

where E is the averaged modulus in the armchair direction ($E_{bi\text{-}armchair}$) or zigzag direction ($E_{bi\text{-}zigzag}$), which can be extracted from the stress-strain curves in Fig. 11. Poisson's ratio v is taken as its average value in the armchair ($v_{armchair}$) and zigzag directions (v_{zigzag}) as shown in Fig. S3 in the supplementary material.

Young's modulus and the ultimate strength extracted from the stress-strain curves of monolayer $MoS_{2x}Te_{2(1-x)}$ under biaxial tension and uniaxial tension at room temperature 300 K are compared in Figs. 13(a) and 13(b). Here, "bi-armchair" and "bi-zigzag" denote the strengths in the armchair and zigzag directions of the nanosheets under biaxial tension, respectively. In Fig. 13(a), we can see that Young's modulus of TMD nanosheets under different loadings generally follows $E_{armchair} > E_{zigzag} > E_{biaxial}$. An exception is that the armchair modulus of $MoS_{1.2}Te_{0.8}$ is slightly smaller than that of zigzag counterparts. Moreover, Young's modulus of monolayer $MoS_{2x}Te_{2(1-x)}$ is found to firstly decrease with the increasing stoichiometric coefficient and thus turn to increase as the stoichiometric coefficient keeps growing. Recalling Eq. (2), the stress equals the total energy divided by the volume. It is found that although the total energy might vary linearly against the stoichiometric coefficient due to the linear changes in the bond energy at a fixed temperature, the volume simultaneously decreases with increasing x as shown in Fig. S1(a) in the supplementary material. These two changes finally lead to a nonlinear variation of Young's modulus of the monolayer $MoS_{2x}Te_{2(1-x)}$ against the stoichiometric coefficient x as shown in Fig. 13(a). As shown in Fig. 13(b), the ultimate strength S of binary TMDs, i.e., MoS_2 and $MoTe_2$ obeys the order of $S_{armchair} > S_{zigzag} > S_{bi\text{-}armchair} \approx S_{bi\text{-}zigzag}$. However, as for the ternary TMDs, the change of ultimate strength under different directions is smaller than that of their binary counterparts. In addition, the ultimate strength of the monolayer $MoS_{2x}Te_{2(1-x)}$ under uniaxial stretching is slightly larger than that under biaxial stretching. Moreover, we can further see from Fig. 13(b) that the influence of the stoichiometric coefficient on the ultimate strength of monolayer $MoS_{2x}Te_{2(1-x)}$ under biaxial loading is similar to its influence on the ultimate strength of monolayer $MoS_{2x}Te_{2(1-x)}$ under uniaxial loading. Comparing the mechanical properties of $MoS_{2x}Te_{2(1-x)}$ nanosheets under different loadings, we see that the nanosheets under biaxial loading possess a smaller Young's modulus and ultimate strength when compared to their counterparts under uniaxial loading.

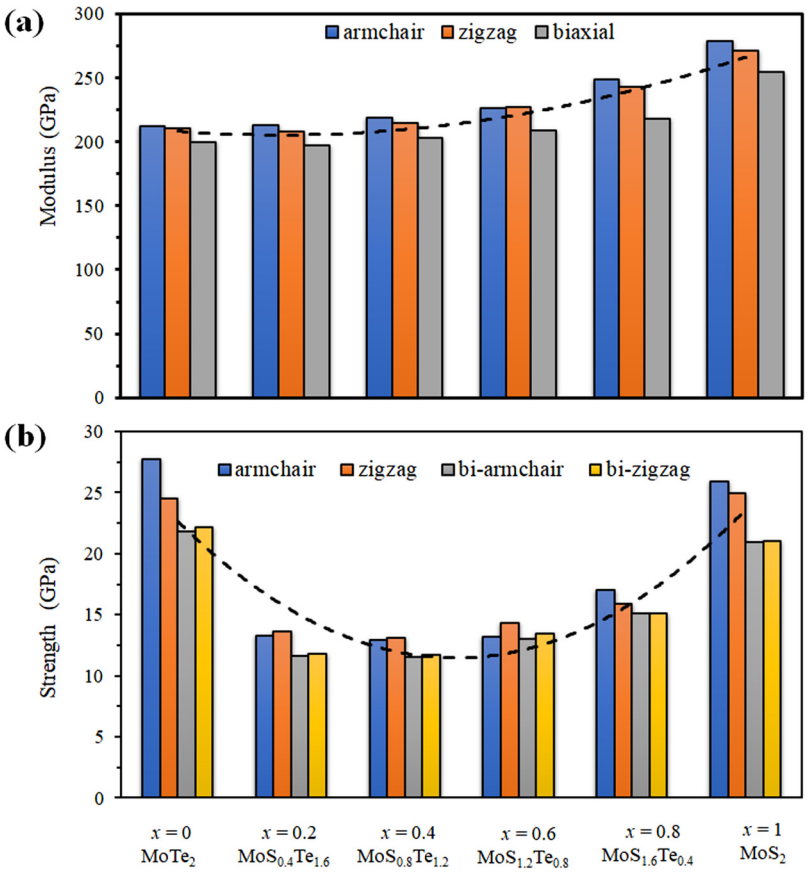

FIG. 13. (a) Young's modulus and (b) ultimate strength of monolayer $MoS_{2x}Te_{2(1-x)}$ nanosheets under uniaxial and biaxial tensile loading. Here, bi-armchair and bi-zigzag, respectively, denote the values in armchair and zigzag directions when the nanosheets are under biaxial tensile loading. The tensile tests are conducted at a temperature of 300 K. The black dashed lines are the polynomial fitting of the average value of modulus and ultimate strength of TMD nanosheets in different loading directions.

IV. CONCLUSIONS

A comprehensive investigation of the mechanical behaviors of monolayer $MoS_{2x}Te_{2(1-x)}$ is conducted by using MD simulations in this paper. The tensile test is employed to the $MoS_{2x}Te_{2(1-x)}$ nanosheets under different temperatures ranging from 100 K to 500 K and with different loading conditions such as uniaxial tension along the armchair/zigzag direction and biaxial tension simultaneously along both directions. During the tensile test simulations, the influence of temperature and loading direction on Young's modulus and fracture behaviors of $MoS_{2x}Te_{2(1-x)}$ nanosheets is well examined.

Young's modulus of monolayer $MoS_{2x}Te_{2(1-x)}$ is found to keep almost unchanged when the stoichiometric coefficient x is in the range of 0–0.4, while it apparently grows when x increases from 0.4 to 1. This result indicates that Young's modulus of $MoTe_2$ nanosheets is insensitive to doping S atoms inside them, while Young's modulus of MoS_2 nanosheets is very sensitive to the doping Te atoms inside the nanosheets. Due to the temperature-induced softening effect, Young's modulus of monolayer $MoS_{2x}Te_{2(1-x)}$ is found to generally decrease as the temperature increases. Moreover, although Young's modulus of monolayer $MoS_{2x}Te_{2(1-x)}$ is isotropic, Young's modulus of $MoS_{2x}Te_{2(1-x)}$ nanosheets under biaxial loading is smaller than that of their counterparts under uniaxial loading.

Different to pristine binary TMD nanosheets, i.e., MoS_2 and $MoTe_2$ possessing a brittle fracture behavior, the present alloyed ternary $MoS_{2x}Te_{2(1-x)}$ nanosheets have a ductile fracture feature. Moreover, the ultimate strength of the alloyed ternary TMDs is found to be much lower than that of the pristine binary TMDs, which is attributed to the uncoordinated deformation caused by stress concentration between Te atoms and nearby S atoms. The ultimate strength of monolayer $MoS_{2x}Te_{2(1-x)}$ is also found to decrease as the temperature increases, which is similarly attributed to the temperature-induced softening effect. In addition, the ultimate strength of monolayer $MoS_{2x}Te_{2(1-x)}$ under biaxial loading is relatively smaller than that under the uniaxial loading. Overall, the present work will not only expand our current knowledge of 2D mechanics but also provide guidelines for the future applications of alloy ternary TMDs.

SUPPLEMENTARY MATERIAL

See the supplementary material for the supplementary figures.

ACKNOWLEDGMENTS

This study was supported by the National Key R&D Program of China (No. 2018YFB1502600) and the National Natural Science Foundation of China (NNSFC) (Nos. 11772106 and 11602074).

REFERENCES

[1]K. S. Novoselov *et al.*, "Electric field effect in atomically thin carbon films," Science **306**(5696), 666–669 (2004).
[2]C. Lee *et al.*, "Measurement of the elastic properties and intrinsic strength of monolayer graphene," Science **321**(5887), 385–388 (2008).
[3]A. A. Balandin *et al.*, "Superior thermal conductivity of single-layer graphene," Nano Lett. **8**(3), 902–907 (2008).
[4]N. M. R. Peres, "The electronic properties of graphene and its bilayer," Vacuum **83**(10), 1248–1252 (2009).
[5]S. Stankovich *et al.*, "Graphene-based composite materials," Nature **442**(7100), 282 (2006).
[6]A. K. Geim and K. S. Novoselov, "The rise of graphene," in *Nanoscience and Technology: A Collection of Reviews From Nature Journals*, edited by P. Rodgers (World Scientific, 2010), pp. 11–19.
[7]M. K. Blees *et al.*, "Graphene kirigami," Nature **524**(7564), 204 (2015).
[8]R. Raccichini *et al.*, "The role of graphene for electrochemical energy storage," Nat. Mater. **14**(3), 271 (2015).
[9]Y. Cao *et al.*, "Unconventional superconductivity in magic-angle graphene superlattices," Nature **556**(7699), 43 (2018).
[10]R. Mas-Balleste *et al.*, "2D materials: To graphene and beyond," Nanoscale **3**(1), 20–30 (2011).
[11]A. Gupta, T. Sakthivel, and S. Seal, "Recent development in 2D materials beyond graphene," Prog. Mater. Sci. **73**, 44–126 (2015).
[12]K. Kam and B. Parkinson, "Detailed photocurrent spectroscopy of the semiconducting group VIB transition metal dichalcogenides," J. Phys. Chem. **86**(4), 463–467 (1982).
[13]V. M. Pereira and A. C. Neto, "Strain engineering of graphene's electronic structure," Phys. Rev. Lett. **103**(4), 046801 (2009).
[14]D. Xiao *et al.*, "Coupled spin and valley physics in monolayers of MoS_2 and other group-VI dichalcogenides," Phys. Rev. Lett. **108**(19), 196802 (2012).
[15]H. Zeng *et al.*, "Valley polarization in MoS_2 monolayers by optical pumping," Nat. Nanotechnol. **7**(8), 490 (2012).
[16]Y. Zhang *et al.*, "Experimental observation of the quantum Hall effect and Berry's phase in graphene," Nature **438**(7065), 201 (2005).
[17]X. Qian *et al.*, "Quantum spin Hall effect in two-dimensional transition metal dichalcogenides," Science **346**(6215), 1344–1347 (2014).
[18]M. Chhowalla, Z. Liu, and H. Zhang, "Two-dimensional transition metal dichalcogenide (TMD) nanosheets," Chem. Soc. Rev. **44**(9), 2584–2586 (2015).
[19]N. Savjani *et al.*, "MoS_2 nanosheet production by the direct exfoliation of molybdenite minerals from several type-localities," RSC Adv. **4**(67), 35609–35613 (2014).
[20]J.-W. Jiang and Y.-P. Zhou, "Parameterization of Stillinger-Weber potential for two-dimensional atomic crystals," in *Handbook of Stillinger-Weber Potential Parameters for Two-Dimensional Atomic Crystals* (IntechOpen, 2017).
[21]B. Tang *et al.*, "Phase-controlled synthesis of monolayer ternary telluride with a random local displacement of tellurium atoms," Adv. Mater. **31**, e1900862 (2019).
[22]J. Zhou *et al.*, "A library of atomically thin metal chalcogenides," Nature **556**(7701), 355–359 (2018).
[23]P. Yu *et al.*, "Metal–semiconductor phase-transition in $WSe_{2\ (1-x)}$ Te_{2x} monolayer," Adv. Mater. **29**(4), 1603991 (2017).
[24]C. Zhang *et al.*, "Charge mediated reversible metal–insulator transition in monolayer $MoTe_2$ and $W_xMo_{1-x}Te_2$ alloy," ACS Nano **10**(8), 7370–7375 (2016).
[25]Y. Gong *et al.*, "Band gap engineering and layer-by-layer mapping of selenium-doped molybdenum disulfide," Nano Lett. **14**(2), 442–449 (2013).
[26]J. Mann *et al.*, "2-dimensional transition metal dichalcogenides with tunable direct band gaps: $MoS_{(2)((1)-x)}$ $Se_{(2)x}$ monolayers," Adv. Mater. **26**(9), 1399–1404 (2014).
[27]X. Duan *et al.*, "Synthesis of $WS_{2x}Se_{2-2x}$ alloy nanosheets with composition-tunable electronic properties," Nano Lett. **16**(1), 264–269 (2016).
[28]S. Zheng *et al.*, "Monolayers of $W_xMo_{1-x}S_2$ alloy heterostructure with in-plane composition variations," Appl. Phys. Lett. **106**(6), 063113 (2015).
[29]V. Kochat *et al.*, "Re doping in 2D transition metal dichalcogenides as a new route to tailor structural phases and induced magnetism," Adv. Mater. **29**(43), 1703754 (2017).
[30]A. Molina-Sánchez and L. Wirtz, "Phonons in single-layer and few-layer MoS_2 and WS_2," Phys. Rev. B **84**(15), 155413 (2011).
[31]S. Plimpton, "Fast parallel algorithms for short-range molecular dynamic," J. Comput. Phys. **117**(1), 1–19 (1995).
[32]J.-W. Jiang, "Misfit strain-induced buckling for transition-metal dichalcogenide lateral heterostructures: A molecular dynamics study," Acta Mech. Solida Sin. **32**(1), 17 (2019).
[33]W. Jiang *et al.*, "Molecular dynamics simulations of single-layer molybdenum disulphide (MoS_2) Stillinger-Weber parametrization, mechanical properties, and thermal conductivity," J. Appl. Phys. **114**(6), 064307 (2013).
[34]J. Zhang, "Phase-dependent mechanical properties of two-dimensional silica films: A molecular dynamics study," Comput. Mater. Sci. **142**, 7–13 (2018).
[35]J. A. Zimmerman *et al.*, "Calculation of stress in atomistic simulation," Modell. Simul. Mater. Sci. Eng. **12**(4), S319 (2004).
[36]H. Qin, X. Pei Q, Y. Liu *et al.*, "Mechanical and thermal properties of MoS_2–WSe_2 lateral heterostructures," Phys. Chem. Chem. Phys. **21**(28), 15845–15853 (2019).
[37]X. Hu, P. Yasaei, J. Jokisaari *et al.*, "Mapping thermal expansion coefficients in freestanding 2D materials at the nanometer scale," Phys. Rev. Lett. **120**(5), 055902 (2018).
[38]M. Born and T. von Kármán, *Über Schwingungen in Raumgittern* (Hirzel, 1912).
[39]J. Zhang and Q. Xiong, "The negative Poisson's ratio in graphene-based carbon foams," Phys. Chem. Chem. Phys. **20**(6), 4597–4605 (2018).
[40]M. Hasanian, B. Mortazavi, A. Ostadhossein *et al.*, "Hydrogenation and defect formation control the strength and ductility of MoS_2 nanosheets: Reactive molecular dynamics simulation," Extreme Mech. Lett. **22**, 157–164 (2018).
[41]W. Jiang J, "Parametrization of Stillinger–Weber potential based on valence force field model: Application to single-layer MoS_2 and black phosphorus," Nanotechnology **26**(31), 315706 (2015).
[42]Z.-D. Sha, Q.-X. Pei, Z. Ding *et al.*, "Mechanical properties and fracture behavior of single-layer phosphorene at finite temperatures," J. Phys. D Appl. Phys. **48**(39), 395303 (2015).
[43]S. Zhao, M. Lu, S. Xue *et al.*, "Large-area synthesis of monolayer $MoTe_x$ Se_{2-x} alloys by chemical vapor deposition," Appl. Phys. Lett. **115**(6), 063105 (2019).
[44]Q. Feng, Y. Zhu, J. Hong *et al.*, "Growth of large-area 2D $MoS_{2\ (1-x)}$ Se_{2x} semiconductor alloys," Adv. Mater. **26**(17), 2648–2653 (2014).
[45]Y. Gan and H. Zhao, "Chirality effect of mechanical and electronic properties of monolayer MoS_2 with vacancies," Phys. Lett. A **378**(38–39), 2910–2914 (2014).
[46]J. Yang *et al.*, "Elastic and electronic tuning of magnetoresistance in $MoTe_2$," Sci. Adv. **3**(12), eaao4949 (2017).
[47]F. Zeng *et al.*, "Electronic structures and elastic properties of monolayer and bilayer transition metal dichalcogenides MX_2 (M=Mo, W; X=O, S, Se, Te): A comparative first-principles study," Chin. Phys. B **24**(9), 097103 (2015).
[48]B. Zillmann *et al.*, "In-plane biaxial compression and tension testing of thin sheet materials," Int. J. Solids Struct. **2015**(66), 111–120 (2015).